PROCEEDINGS OF SPIE

SPIEDigitalLibrary.org/conference-proceedings-of-spie

Rapid microfabrication of helical structures for industrial applications

Cheng, He, Golvari, Pooria, Xia, Chun, Sun, Mingman, Zhang, Meng, et al.

He Cheng, Pooria Golvari, Chun Xia, Mingman Sun, Meng Zhang, Stephen M. Kuebler, Xiaoming Yu, "Rapid microfabrication of helical structures for industrial applications," Proc. SPIE 12012, Advanced Fabrication Technologies for Micro/Nano Optics and Photonics XV, 1201205 (5 March 2022); doi: 10.1117/12.2608940



Event: SPIE OPTO, 2022, San Francisco, California, United States

Rapid microfabrication of helical structures for industrial applications

He Cheng^a, Pooria Golvari^b, Chun Xia^a, Mingman Sun^c, Meng Zhang^c, Stephen M. Kuebler^{abd}, Xiaoming Yu^a

aCREOL, The College of Optics and Photonics, University of Central Florida, Orlando, Florida 32816, USA;
 bDepartment of Chemistry, University of Central Florida, Orlando, Florida 32816, USA;
 cDepartment of Industrial and Manufacturing Systems Engineering, Kansas State University, Manhattan, Kansas 66506, USA;
 dDepartment of Material Science and Engineering, University of Central Florida, Orlando, Florida, 32816, USA

ABSTRACT

Helical structures exhibit novel optical and mechanical properties and are commonly used in different fields such as metamaterials and microfluidics. A few methods exist for fabricating helical microstructures, but none of them has the throughput or flexibility required for patterning large surface areas with tunable pitch. In this paper, we report a method for fabricating helical structures with high-throughput and adjustable form based on multiphoton polymerization (MPP) using single-exposure, three-dimensionally structured, self-accelerating, axially tunable light-fields. The light-fields are generated as a superposition of high-order Bessel modes and have a closed-form expression relating the design of the phase mask to the rotation rate of the beam. The method is used to fabricate helices with different pitches and handedness in the material SU-8. Beam splitting and galvo-scanning can be implemented in the system. The fabrication of helical matrices is demonstrated. Compared to point-by-point scanning, our method increases the fabrication speed by two orders of magnitude, paving the way for adopting MPP for mass production of functional devices in many industrial applications. **Keywords:** Multiphoton polymerization; spatial beam shaping; volumetric microfabrication.

1. INTRODUCTION

In the last two decades, helical microstructures have drawn increased attention because they exhibit unique optical and mechanical properties in various fields. Metamaterials with helical structures show novel optical properties, like circular dichroism [1], optical activity [2], and negative refractive index [3,4]. Prototype optical devices utilizing helical microstructures such as broadband circular polarizers [2,5], circular polarization converters [6], and wave plates [7] have been demonstrated. Helical microchannels are used as microfluidic mixers [8,9]. Magnetic micro-helices driven by magnetic field are used as micro-robots [10,11], with potential applications in medicine. Helical microstructures could also have useful applications as microfluidic sensors [12], heat diffusers [13,14], and scaffolds for growing cells [15].

Producing helical structures requires nonplanar fabrication methods such as multiphoton polymerization (MPP). MPP is a direct laser writing technique that is increasingly used [1,5,6,16–20] because it provides a means for creating almost arbitrarily shaped, three-dimensional (3D) structures with high resolution. However, MPP is time-consuming due to the point-by-point writing strategy. It often requires hours or even days to fabricate a part depending on the size and resolution. The slow fabrication speed of conventional MPP is the key factor that limits its wider application for industrial manufacturing. One approach for increasing fabrication speed is to turn the point-by-point scanning into a volumetric process by spatially shaping the laser beam so that one entire layer or even the complete structure could be fabricated with a single exposure. Layer-by-layer fabrication of various extruded tube-like 3D structures has been demonstrated by focusing shaped Bessel beam [21–25]. The fabrication is achieved by scanning the focused beam along the optical axis, but the increase in throughput is limited because axial scanning is still needed. Volumetric fabrication with single exposure has also been demonstrated, including the fabrication of high-aspect-ratio structures using Bessel- [26,27] and axilens beams [28]. However, the shape of the structures is limited by the needle-like focal shape and thus lacks variety. Vortex beams have been used to fabricate 3D helical structures with limited aspect ratios [29–31]. For good optical and mechanical functionality, helical structures are often required to have multiple pitches and high aspect ratios, such as those used as microfluidic mixers [8,9] and helical structures used in metamaterials [2,5,16,32,33]. However, methods reported in Ref. [29–31] only achieved low aspect-ratio helical structure with less than one pitch. So far, no method has the throughput required for fabricating over a large area with tall helices that have multiple variable pitches.

Advanced Fabrication Technologies for Micro/Nano Optics and Photonics XV, edited by Georg von Freymann, Eva Blasco, Debashis Chanda, Proc. of SPIE Vol. 12012, 1201205 · © 2022 SPIE · 0277-786X · doi: 10.1117/12.2608940

In this work, we report a volumetric fabrication approach based on MPP with single-exposure using a new class of self-accelerating beams (SABs) with rotating intensity distribution [34–37]. The proposed SABs are based on the superposition of two high-order Bessel beam modes. Compared to the existing radially self-accelerating beams with constant rotation rate, the proposed beams feature tunable angular acceleration (variable pitch), which means the rotation rate (and hence pitch) can be tailored to follow a nearly arbitrary profile within the limit of optical arrangement, while other SABs with angular acceleration reported in Ref. [38–40] follow a specific equation with single tuning parameter. We have developed an analytical model to describe the generation and propagation of the SABs. A closed-form solution for the intensity distribution and rotation rate are derived, thus a direct calculation of computer-generated hologram (CGH) for the SABs can be performed. The analytic model makes it easier to synthesize 3D beams and is an improvement on the iterative algorithms used by others. Micro-helices with constant and varying pitches are fabricated with a single exposure in the forms of individual helices and matrices of helices. With optimization, this method can be used to increase throughput by more than two orders of magnitude over conventional MPP and paves the way for mass microfabrication of helical structures for many industrial applications, including metamaterials, microfluidics and biomaterials.

2. THEORY AND CGH DESIGN

In this work, we apply CGH on a phase-only SLM to generate the SABs. The foundation of our SABs is the superposition of two high-order Bessel beam modes. The Bessel-beam phase (BBP, Fig. 1) of two Bessel beam modes with orders l and m can be expressed in terms of a common axicon phase component $k_{\perp}r$ and their individual azimuthal phase components $l\theta$ and $m\theta$ [41–44]:

$$BBP_l = -k_{\perp}r + l\theta, \qquad BBP_m = -k_{\perp}r + m\theta.$$
 (1)

Inspired by the concept of geometrical r-z mapping relationship [45], we introduce a rotation-tuning function v(r) to modulate the phase along the radial direction. This extra phase term, which we call "radial phase modulation" (RPM, Fig. 1), is written as:

$$RPM_l = -RPM_m = -\frac{l-m}{2}v(r)r. \tag{2}$$

The superposition of these two components gives a transmittance function $T(r,\theta) = \exp(-i(BBP_l + RPM_l)) + \exp(-i(BBP_m + RPM_m))$ which is the desired CGH. As $T(r,\theta)$ has both phase and amplitude information, in order to display it on the phase-only SLM, we use a phase encoding method that is based on a pair of complementary "binary amplitude masks" (BAMs, Fig. 1) with checkerboard patterns [46]. After encoding, the phase becomes:

$$\varphi(r,\theta) = (BBP_l + RPM_l) \times BAM_l + (BBP_m + RPM_m) \times BAM_m. \tag{3}$$

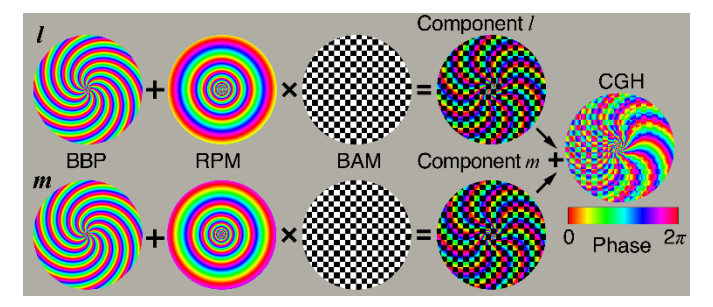


Figure 1. Design of a computer-generated hologram (CGH). Phase order l = -10, m = -9.

The encoded phase $\varphi(r,\theta)$ is displayed on the SLM as it is illuminated with a Gaussian beam. The beam reflected off SLM is sent into a 4-f system with a low-pass filter applied at the Fourier plane. Using Fresnel diffraction theory and the stationary phase method [40,47,48], we can derive a closed-form solution for the intensity distribution at point (r, θ, z) after image plane:

$$I(r,\theta,z)_{l+m} = ze^{-2\frac{k'_{\perp}^{2}}{k^{2}w_{0}^{2}}z^{2}} \left\{ |C_{l}|^{2}J_{l}^{2}(k'_{\perp}r) + |C_{m}|^{2}J_{m}^{2}(k'_{\perp}r) + 2|C_{l}||C_{m}|J_{l}(k'_{\perp}r)J_{m}(k'_{\perp}r) \right\} \times \cos\left[(l-m)\left(\theta + Mv\left(M\frac{k'_{\perp}}{k}z\right)\frac{k'_{\perp}}{k}z\right) + \theta_{lm} \right],$$

$$(4)$$

where M is the demagnification rate of 4-f system, $w_0' \equiv w_0/M$ is the normalized Gaussian beam waist, and $k_\perp' \equiv Mk_\perp$. C_l , C_m and θ_{lm} are constants. The term $z \exp\left[-2k_\perp'^2z^2/(k^2w_0'^2)\right]$ in Eq. (4) describes the intensity variation along the z-axis, and it means that the depth of focus is limited by the size of Gaussian illumination. To study the rotation of the intensity profile on a transverse plane, we temporarily drop this term. The rest of the terms describe an intensity distribution that is rotating along z-axis, and the rotation rate could be expressed as

$$\omega(z) \equiv \frac{d\theta}{dz} = -\frac{k_{\perp}}{k} M^2 v' \left(M^2 \frac{k_{\perp}}{k} z \right) z - \frac{k_{\perp}}{k} M^2 v \left(M^2 \frac{k_{\perp}}{k} z \right), \tag{5}$$

where v' represents the first derivative of v with respect to z. Equation (A34) establishes a "forward" relationship between the rotation rate $\omega(z)$ and rotation tunning function v(r). Treating function v(r) as unknown, we can rewrite Eq. (5) as an ordinary linear differential equation which has the following general solution

$$v(r) = \frac{1}{r} \int -M^{-2} \frac{k}{k_{\perp}} \omega \left(M^{-2} \frac{k}{k_{\perp}} r \right) dr. \tag{6}$$

Equation (6) provides a "reverse" relationship between $\omega(z)$ and v(r) and is the key to generating SABs in this work. This equation can be solved analytically or numerically to obtain a CGH that produces a beam with a specific rotation profile described by $\omega(z)$. This makes it possible to tailor the SAB's rotation on-demand without time-consuming phase-retrieval algorithms [51]. Using a similar method, the propagation of the proposed SABs through the planer interface can be derived. We found that the refraction from the interface will not affect the transverse intensity distribution of the SABs; only the rotation rate will be decreased once propagated into a medium with higher refractive index.

3. EXPERIMENTAL RESULTS

In the experiment, the light-source is a femtosecond laser (Pharos, Light Conversion) that generates pulses having a temporal full-width at half-maximum (FWHM) of 170 fs, center wavelength of $\lambda_0 = 1030$ nm, and repetition rate of 100 kHz. The output beam is frequency-doubled by a beta barium borate (BBO) crystal, expanded and collimated, and sent to a spatial light modulator (SLM), which is a reflecting, phase-only, liquid-crystal-on-silicon device (Meadowlark Optics, 1920×1150 pixels, 256 gray levels, 9.2 µm pixel-pitch). CGHs generated with the proposed method are displayed on the SLM. The beam is reflected off the SLM and directed into a 4-f system composed of a plano-convex lens (f = 750 mm) and an objective lens ($10 \times$, NA = 0.3, focal length = 18 mm) and then spatially filtered by an iris placed at the Fourier plane of the 4-f system. The optical field at the focal plane of the objective lens is a demagnified replica of that formed on the SLM. The SABs generated by the proposed method are measured in free space to validate the theory. A

CMOS camera with a $20 \times$ objective lens shown in Fig. 1a is mounted on a motorized stage to image a series of transverse (x-y) intensity distributions at positions z along the optical axis (Figs. 2d).

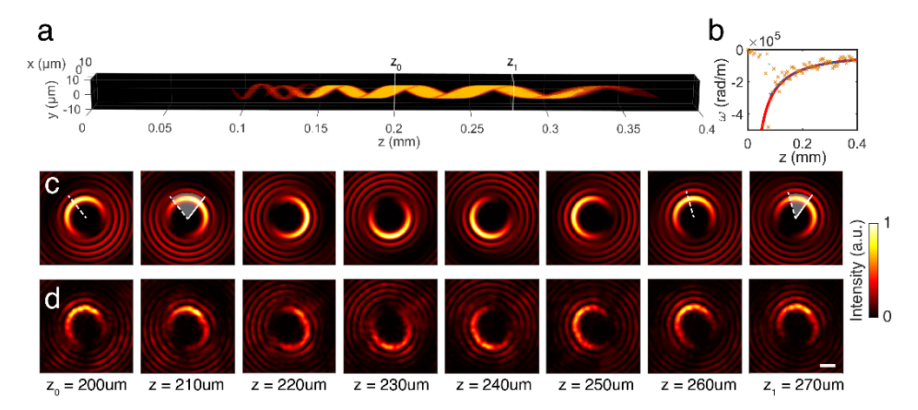


Figure 2. Comparison of simulated and measured SAB with decelerated rotation rate. Phase order l = -10 and m = -9. (a) Iso-intensity contours of simulated SABs in air. The threshold intensity (normalized) is set to 0.5. (c) Simulated and (d) measured x-y intensity distribution. Scale bar represents 5 μ m. (b) Rotation rate ω along optical axis. Red curves, designed profile; orange points, measured data; blue dot, simulation results.

One example of an SAB shown in Figure 2 has decreasing rotation rate $\omega=-25.13z^{-1}$ rad/m in air and topological charges l=-10, m=-9 and $k_\perp=6.6\times10^4$ m⁻¹. The white sector shapes in Fig. 2c show that $\Delta\alpha$ has reduced from z=210 mm to z=270 mm. Experimental measurements (Fig. 2d) of the transverse intensity profile on the x-y plane shows good agreement with the simulation results (Fig. 2c) in spite of some distortions caused by aberrations in the optical system. The SAB has a "C" shape transverse intensity profile with a radius of \sim 5 μ m. The SAB shows a long depth of focus, greater than 300 μ m. In space, the intensity distribution of the SAB has a helical shape that resembles a twisted strap. We measured the rotation by extracting the directional angle α from x-y intensity profile of SAB and calculating the rotation rate by $\omega(z) = \Delta\alpha/\Delta z$. As shown in Fig. 2b, the rotation rate matches the theory. The deviation is due to the aforementioned distortions in experimentally generated beam profiles. We also observe a deviation from the "C" shape in x-y plane intensity distribution both experimentally and in simulation at the beginning of the SAB where the rotation rate exceeds 2×10^5 rad/m. This is shown in Fig. 2a on the left of the SAB. Here the beam appears as a "double helix" (left side of Fig. 2a) and indicates the limit of the highest rotation rate that can be obtained with this method. By using Eq. (6), we are able to obtain SABs with different rotation rates along the optical axis as will be demonstrated in the fabrication results.

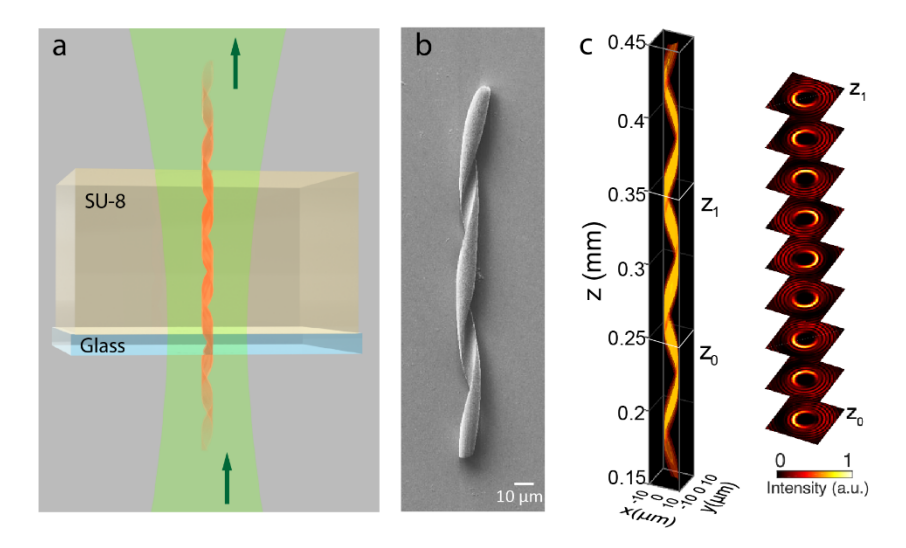


Figure 3. Volumetric fabrication of micro-helix with a single exposure of SAB. (a) Illustration of exposure in the SU-8 sample. The green arrow shows the beam propagation direction. (b) SEM images of a fabricated single helix. (c) Simulation of the SAB used in fabrication in (b).

Equation (6) was used to design CGHs that generate SABs for fabricating helices in SU-8. The CGHs have phase order (l, m) = (-10, -9) and $k_{\perp} = 6.6 \times 10^4$ m⁻¹. The demagnified beam is directed into a layer of photoresist (SU-8 2075, Kayaku Advanced Materials) that was spin-coated on a glass substrate (Fig. 3a) and baked prior to exposure to remove the solvent. Each helix was patterned with static exposure (no scanning) and an exposure time of less than 0.15 ms. After exposure, the sample is baked to activate cross-linking and developed in propylene glycol methyl ether acetate (PGMEA) to remove unexposed material. The resulting structures were imaged by scanning electron microscopy (SEM). The results are shown in Fig. 3. Fresnel diffraction theory is used to simulate the SABs in photoresist. An example of an iso-intensity contour of the simulated SABs used in fabrication is plotted in Fig. 3c together with cross-sections of the intensity distribution. The SAB demonstrated here features a constant rotation rate along the optical axis. Figures 3b and 3c show a comparison between the simulated beam shape and fabricated micro-helices. The length of the helix is limited by the thickness of the spin-coated SU-8 layer. Because of the high aspect-ratio, a single helix does not withstand the capillary force during development and is found lying down on the glass substrate.

By performing a series of single exposures with lateral translation (Fig. 4e), helical matrices can be fabricated. Figure 4 shows several matrices, each consisting of 30 × 30 helices with a certain pitch and handedness. The fabrication time for each matrix is approximately 15 min, and most of the time is spent on translating the sample. In terms of fabrication volume per unit time, the method reported here is more than 100 times faster than point-by-point scanning for similar structures reported in [1]. The fabrication time could be further reduced by adding a galvanometer scanner to increase the speed of lateral scanning. The helical structures shown in Fig. 4 can be used as metamaterials at terahertz frequencies [58,59]. Further reduction in pitch can be achieved by tighter focusing (which may require the use of vectorial diffraction theories) and will enable application at optical frequencies.

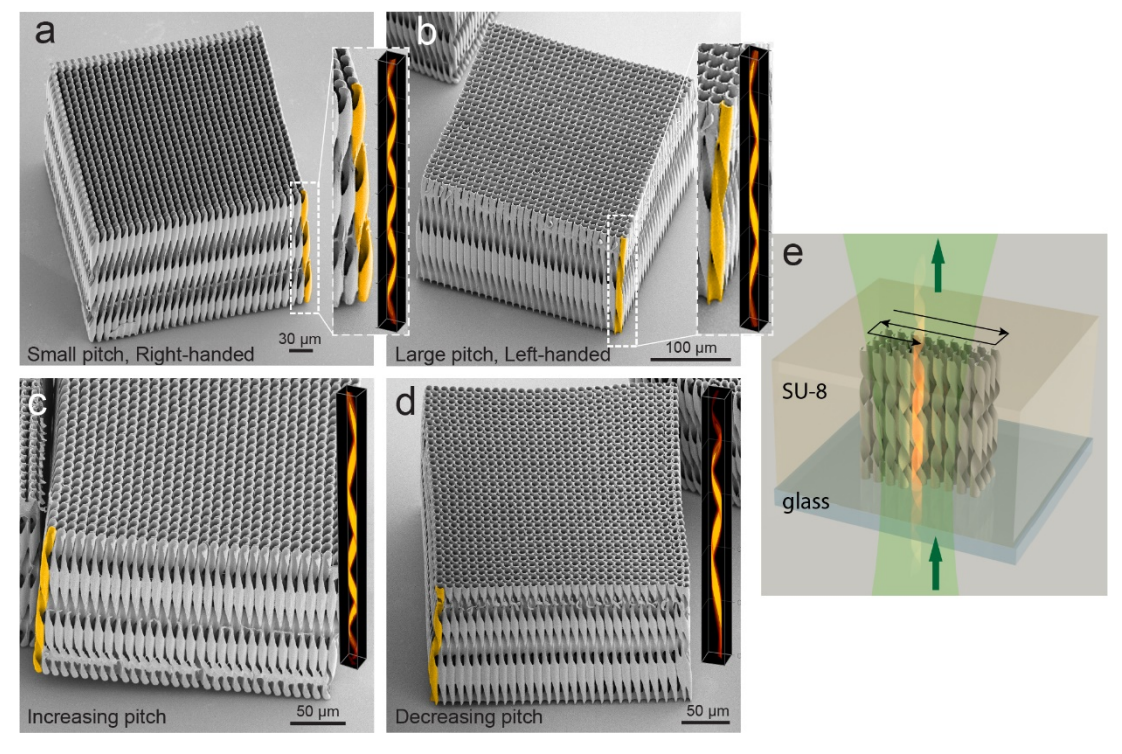


Figure 4. Matrices of various helical structures fabricated by a combination of exposure and linear translation.

4. CONCLUSION

We have demonstrated a method for rapid microfabrication of helical structures with a tunable axial pitch by proposing a new class of SABs and adapting them to MPP. The SABs are based on the superposition of high-order Bessel modes and form non-diffracting transverse intensity profiles that rotate along the optical axis. A closed-form expression was derived that can be used to directly synthesize targeted CGH and SAB without resorting to iterative algorithms. SABs can be generated with independently adjustable transverse width and rotational pitch. Single micro-helices can be fabricated with a single exposure of SAB. Matrices of helices with various pitch and handedness were fabricated rapidly in SU-8 with

good agreement with the beam shapes. The approach reduced fabrication time by two orders of magnitude relative to conventional point-by-point scanning MPP. As a first step toward full volumetric fabrication, our method addresses the low throughput issue of MPP and represents a leap forward towards mass microfabrication in industrial applications.

Acknowledgement

This material is based partly upon work supported by the National Science Foundation under Grants No. 1711356 and 1846671.

REFERENCES

- 1. M. Thiel, M. Decker, M. Deubel, M. Wegener, S. Linden, and G. von Freymann, "Polarization Stop Bands in Chiral Polymeric Three-Dimensional Photonic Crystals," Adv. Mater. 19(2), 207–210 (2007).
- 2. J. K. Gansel, M. Thiel, M. S. Rill, M. Decker, K. Bade, V. Saile, G. von Freymann, S. Linden, and M. Wegener, "Gold Helix Photonic Metamaterial as Broadband Circular Polarizer," Science **325**(5947), 1513–1515 (2009).
- 3. J. B. Pendry, "A Chiral Route to Negative Refraction," Science **306**(5700), 1353–1355 (2004).
- 4. E. Plum, J. Zhou, J. Dong, V. A. Fedotov, T. Koschny, C. M. Soukoulis, and N. I. Zheludev, "Metamaterial with negative index due to chirality," Phys. Rev. B **79**(3), 035407 (2009).
- 5. J. K. Gansel, M. Latzel, A. Frölich, J. Kaschke, M. Thiel, and M. Wegener, "Tapered gold-helix metamaterials as improved circular polarizers," Appl. Phys. Lett. **100**(10), 101109 (2012).
- 6. J. Kaschke, L. Blume, L. Wu, M. Thiel, K. Bade, Z. Yang, and M. Wegener, "A Helical Metamaterial for Broadband Circular Polarization Conversion," Adv. Opt. Mater. 3(10), 1411–1417 (2015).
- 7. C. Wu, H. Li, X. Yu, F. Li, H. Chen, and C. T. Chan, "Metallic Helix Array as a Broadband Wave Plate," Phys. Rev. Lett. **107**(17), 177401 (2011).
- 8. M. K. S. Verma, S. R. Ganneboyina, Rakshith, and A. Ghatak, "Three-Dimensional Multihelical Microfluidic Mixers for Rapid Mixing of Liquids," Langmuir **24**(5), 2248–2251 (2008).
- 9. C. Shan, F. Chen, Q. Yang, Z. Jiang, and X. Hou, "3D Multi-Microchannel Helical Mixer Fabricated by Femtosecond Laser inside Fused Silica," Micromachines 9(1), 29 (2018).
- 10. S. Tottori, L. Zhang, F. Qiu, K. K. Krawczyk, A. Franco-Obregon, and B. J. Nelson, "Magnetic helical micromachines: Fabrication, controlled swimming, and cargo transport," Adv. Mater. **24**(6), 811–816 (2012).
- 11. L. Zhang, J. J. Abbott, L. Dong, B. E. Kratochvil, D. Bell, and B. J. Nelson, "Artificial bacterial flagella: Fabrication and magnetic control," Appl. Phys. Lett. **94**(6), 3–5 (2009).
- 12. W. Li, G. Huang, J. Wang, Y. Yu, X. Wu, X. Cui, and Y. Mei, "Superelastic metal microsprings as fluidic sensors and actuators," Lab Chip **12**(13), 2322 (2012).
- 13. M. I. Hussain, G. H. Lee, and B. Engineering, "Numerical thermal analysis of helical-shaped heat exchanger to improve thermal stratification inside solar," Proc. Int. Conf. Agric. Eng. Zurich 6(10), 6–10 (2014).
- 14. E. S. Shukri, "Numerical Comparison of Temperature Distribution in an Annular Diffuser Fitted with Helical Screw-Tape Hub and Pimpled Hub," Energy Procedia **141**, 625–629 (2017).
- 15. A. V. Do, B. Khorsand, S. M. Geary, and A. K. Salem, "3D Printing of Scaffolds for Tissue Regeneration Applications," Adv. Healthc. Mater. 4(12), 1742–1762 (2015).
- 16. M. Thiel, M. S. Rill, G. von Freymann, and M. Wegener, "Three-Dimensional Bi-Chiral Photonic Crystals," Adv. Mater. **21**(46), 4680–4682 (2009).
- 17. J. Kaschke and M. Wegener, "Gold triple-helix mid-infrared metamaterial by STED-inspired laser lithography," Opt. Lett. **40**(17), 3986 (2015).
- 18. Y. Liu, J. Campbell, O. Stein, L. Jiang, J. Hund, and Y. Lu, "Deformation Behavior of Foam Laser Targets Fabricated by Two-Photon Polymerization," Nanomaterials **8**(7), 498 (2018).
- 19. G. Kumi, C. O. Yanez, K. D. Belfield, and J. T. Fourkas, "High-speed multiphoton absorption polymerization: Fabrication of microfluidic channels with arbitrary cross-sections and high aspect ratios," Lab Chip **10**(8), 1057–1060 (2010).
- 20. S. Kawata, H. B. Sun, T. Tanaka, and K. Takada, "Finer features for functional microdevices," Nature **412**(6848), 697–698 (2001).
- 21. L. Yang, S. Ji, K. Xie, W. Du, B. Liu, Y. Hu, J. Li, G. Zhao, D. Wu, W. Huang, S. Liu, H. Jiang, and J. Chu, "High efficiency fabrication of complex microtube arrays by scanning focused femtosecond laser Bessel beam

- for trapping/releasing biological cells," Opt. Express 25(7), 8144 (2017).
- 22. S. Ji, L. Yang, C. Zhang, Z. Cai, Y. Hu, J. Li, D. Wu, and J. Chu, "High-aspect-ratio microtubes with variable diameter and uniform wall thickness by compressing Bessel hologram phase depth," Opt. Lett. **43**(15), 3514 (2018).
- 23. S. Ji, L. Yang, Y. Hu, J. Ni, W. Du, J. Li, G. Zhao, D. Wu, and J. Chu, "Dimension-Controllable Microtube Arrays by Dynamic Holographic Processing as 3D Yeast Culture Scaffolds for Asymmetrical Growth Regulation," Small 13(34), 1701190 (2017).
- 24. L. Yang, D. Qian, C. Xin, Z. Hu, S. Ji, D. Wu, Y. Hu, J. Li, W. Huang, and J. Chu, "Two-photon polymerization of microstructures by a non-diffraction multifoci pattern generated from a superposed Bessel beam," Opt. Lett. 42(4), 743 (2017).
- L. Yang, D. Qian, C. Xin, Z. Hu, S. Ji, D. Wu, Y. Hu, J. Li, W. Huang, and J. Chu, "Direct laser writing of complex microtubes using femtosecond vortex beams," Appl. Phys. Lett. 110(22), 221103 (2017).
- 26. H. Cheng, C. Xia, M. Zhang, S. M. Kuebler, and X. Yu, "Fabrication of high-aspect-ratio structures using Bessel-beam-activated photopolymerization," Appl. Opt. **58**(13), D91 (2019).
- 27. J. Jezek, T. Cizmár, V. Nedela, and P. Zemánek, "Formation of long and thin polymer fiber using nondiffracting beam.," Opt. Express **14**(19), 8506–8515 (2006).
- 28. D. Pan, B. Xu, S. Liu, J. Li, Y. Hu, D. Wu, and J. Chu, "Amplitude-phase optimized long depth of focus femtosecond axilens beam for single-exposure fabrication of high-aspect-ratio microstructures," Opt. Lett. **45**(9), 2584 (2020).
- 29. S.-J. Zhang, Y. Li, Z.-P. Liu, J.-L. Ren, Y.-F. Xiao, H. Yang, and Q. Gong, "Two-photon polymerization of a three dimensional structure using beams with orbital angular momentum," Appl. Phys. Lett. **105**(6), 061101 (2014).
- 30. J. Ni, C. Wang, C. Zhang, Y. Hu, L. Yang, Z. Lao, B. Xu, J. Li, D. Wu, and J. Chu, "Three-dimensional chiral microstructures fabricated by structured optical vortices in isotropic material," Light Sci. Appl. 6(7), e17011–e17011 (2017).
- 31. Y. Li, L. Liu, D. Yang, Q. Zhang, H. Yang, and Q. Gong, "Femtosecond laser nano/microfabrication via three-dimensional focal field engineering," in *Laser-Based Micro- and Nanoprocessing XI* (2017), **10092**(May), p. 100920B.
- 32. J. Kaschke, J. K. Gansel, and M. Wegener, "On metamaterial circular polarizers based on metal N-helices," Opt. Express **20**(23), 26012 (2012).
- 33. J. K. Gansel, M. Wegener, S. Burger, and S. Linden, "Gold helix photonic metamaterials: A numerical parameter study," Opt. Express **18**(2), 1059 (2010).
- 34. C. Vetter, T. Eichelkraut, M. Ornigotti, and A. Szameit, "Optimization and control of two-component radially self-accelerating beams," Appl. Phys. Lett. **107**(21), 211104 (2015).
- 35. C. Vetter, T. Eichelkraut, M. Ornigotti, and A. Szameit, "Generalized Radially Self-Accelerating Helicon Beams," Phys. Rev. Lett. **113**(18), 183901 (2014).
- 36. R. Rop, A. Dudley, C. López-Mariscal, and A. Forbes, "Measuring the rotation rates of superpositions of higher-order Bessel beams," J. Mod. Opt. **59**(3), 259–267 (2012).
- 37. R. Vasilyeu, A. Dudley, N. Khilo, and A. Forbes, "Generating superpositions of higher–order Bessel beams," Opt. Express 17(26), 23389 (2009).
- 38. C. Schulze, F. S. Roux, A. Dudley, R. Rop, M. Duparré, and A. Forbes, "Accelerated rotation with orbital angular momentum modes," Phys. Rev. A **91**(4), 043821 (2015).
- 39. C. Vetter, A. Dudley, A. Szameit, and A. Forbes, "Real and virtual propagation dynamics of angular accelerating white light beams," Opt. Express **25**(17), 20530 (2017).
- 40. J. Webster, C. Rosales-Guzmán, and A. Forbes, "Radially dependent angular acceleration of twisted light," Opt. Lett. **42**(4), 675 (2017).
- 41. A. Vasara, J. Turunen, and A. T. Friberg, "Realization of general nondiffracting beams with computer-generated holograms," J. Opt. Soc. Am. A 6(11), 1748 (1989).
- 42. N. Chattrapiban, E. A. Rogers, D. Cofield, W. T. Hill, III, and R. Roy, "Generation of nondiffracting Bessel beams by use of a spatial light modulator," Opt. Lett. **28**(22), 2183 (2003).
- 43. C. Paterson and R. Smith, "Higher-order Bessel waves produced by axicon-type computer-generated holograms," Opt. Commun. **124**(1–2), 121–130 (1996).
- 44. X. Yu, A. Todi, and H. Tang, "Bessel beam generation using a segmented deformable mirror," Appl. Opt. **57**(16), 4677 (2018).

- 45. H. Cheng, C. Xia, S. M. Kuebler, and X. Yu, "Aberration correction for SLM-generated Bessel beams propagating through tilted interfaces," Opt. Commun. **475**(June), 126213 (2020).
- 46. O. Mendoza-Yero, G. Mínguez-Vega, and J. Lancis, "Encoding complex fields by using a phase-only optical element," Opt. Lett. **39**(7), 1740 (2014).